Bandgap Restructuring of the Layered Semiconductor Gallium Telluride in Air

*Jose J. Fonseca, Sefaattin Tongay, Mehmet Topsakal, Annabel R. Chew, Alan J. Lin, Changhyun Ko, Alexander V. Luce, Alberto Salleo, Junqiao Wu, and Oscar D. Dubon**

Layered semiconductors such as the transition-metal dichalcogenide (TMD) MoS_2 have gained much attention as test beds for studies of 2D phenomena in the solid state as well as for alternative electronic device architectures.[1–7] The layered nature of TMDs enables novel, otherwise unavailable approaches to address longstanding challenges in semiconductor science, including doping and surface pinning of the Fermi level, as the natural self-termination of each layer suppresses the formation of electronic surface states. Importantly, the surface offers a direct route to access and modify the bulk properties of these materials. Here we show that in the layered chalcogenide GaTe exposure to air induces a large reduction of its band gap from 1.65 to below 0.8 eV. Oxygen chemisorbed to the Te-terminated surfaces produces significant conduction band restructuring. Remarkably, such chemisorption process results in a crystal structure that is at once layered and disordered.

Gallium telluride can possess thickness-dependent properties similar to TMDs.[1,8–10] It is a layered, direct-bandgap semiconductor, typically p-type with a gap of ≈1.65 eV at room temperature[11,12] and with potential applications that range from radiation detectors to optoelectronic devices.[13–17] Gallium telluride has a monoclinic structure (C2/m space group) with a metastable hexagonal phase.[18–21] Its layers are composed of a Te—Ga—Ga—Te assembly along the *c*-axis (normal to the layer). In this study we use the ambient (air) as a source of intercalating adsorbate and monitor changes over time in the optical, electrical, chemical, and structural properties of GaTe.

J. J. Fonseca, Dr. S. Tongay,[+] A. J. Lin, Dr. C. Ko, Dr. A. V. Luce, Prof. J. Wu, Prof. O. D. Dubon
Department of Materials Science and Engineering
University of California
Berkeley, CA 94720, USA
E-mail: oddubon@berkeley.edu

J. J. Fonseca, A. J. Lin, Dr. A. V. Luce, Prof. J. Wu, Prof. O. D. Dubon
Materials Sciences Division
Lawrence Berkeley National Laboratory
Berkeley, CA 94720, USA

Dr. M. Topsakal
Department of Chemical Engineering and Materials Science
University of Minnesota
MN 55455, USA

A. R. Chew, Prof. A. Salleo
Department of Materials Science and Engineering
Stanford University
Palo Alto, CA 94305, USA

[+]Present address: Department of Materials Science and Engineering, Arizona State University, Tempe, Arizona 85287, USA

DOI: 10.1002/adma.201601151

Figure 1a shows the room-temperature, optical absorption spectra of bulk GaTe (p-type, 2.5×10^{16} cm^{-3}, 20 cm^2 V^{-1} s^{-1}) with increasing time of exposure to air. For an as-cleaved crystal the absorption edge corresponding to the direct band-to-band transition overlapping an excitonic absorption peak is observed at ≈1.65 eV. After exposure to air, strong absorption of photons with energies below the band edge occurs, and a new absorption edge emerges. The square root of absorbance versus photon energy shows a linear relationship (inset, Figure 1a), characteristic of an indirect band-to-band transition.[22] Extrapolation of this new edge yields an onset of absorption of 0.77 eV, less than half of the bandgap of pristine GaTe. This new absorption edge cannot be attributed to the formation of the common oxide-decomposition products TeO_2 or Ga_2O_3 as their bandgaps are ≈3.8 eV and 4.9 eV, respectively.[23,24]

Loss of the photoluminescence (PL) signal as the result of the exposure to air is seen in Figure 1b. Exposure times longer than 20 d lead to the complete disappearance of the peak. As expected for an indirect-bandgap semiconductor, the transformed layer does not show any photoluminescence in the photon energy range of 0.68–2.3 eV. Loss of the PL signal from pristine GaTe over time and the emergence of a sub-bandgap absorption edge are consistent with the formation of an indirect bandgap material at the surface that grows over time. We note that the PL and optical absorption spectra associated with as-cleaved GaTe reappear in samples upon removal of a surface layer via exfoliation.

Figure 1c shows the evolution of the Raman spectrum of exfoliated, or cleaved, single crystals of GaTe after being exposed to air. The peaks at 112, 117, 164, 177, 210, 270, and 283 cm^{-1} observed in the as-cleaved sample have been previously identified for monoclinic GaTe.[25–27] With an extended exposure to air, two new broad peaks at 131 and 145 cm^{-1} grow until they dominate the Raman spectrum. There is an additional weak peak at around 280 cm^{-1}. Although these new peaks have not been identified for GaTe, they have been attributed to defects or disorder since the peaks are broad.[17,28] As with the PL and optical absorption spectra, the Raman spectrum associated with as-cleaved GaTe reappears in samples upon removal of a surface layer via exfoliation. We note that a Raman spectrum such as the one in Figure 1c (blue curve) was measured in thin, multilayered crystals.[14] It is speculated that such a change in the Raman spectrum may be related to a reduced thickness effect; however, no physical basis for this explanation is provided. We will show that this trio of Raman peaks can arise from an oxygen-chemisorbed phase.

In order to confirm that the aforementioned changes are caused by air, samples were stored in vacuum (<1×10^{-7} Torr) for two weeks and characterized; all spectra (not shown) indicate no change from the as-cleaved condition and can be assigned

© 2016 WILEY-VCH Verlag GmbH & Co. KGaA, Weinheim

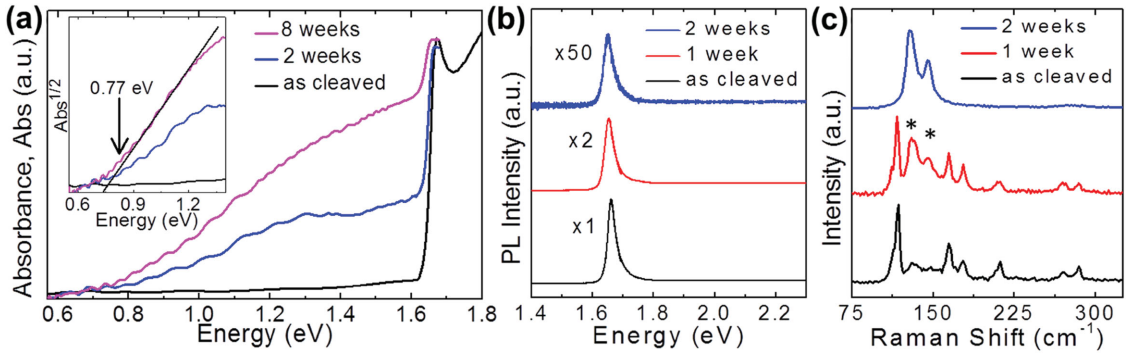

Figure 1. a) Optical absorption spectra of GaTe at a different exposure time to air: as-cleaved (black), two weeks (blue) and eight weeks (magenta). The excitonic absorption peak is observed around 1.65 eV. Oscillations in the sub-bandgap absorption arise from Fabry–Pérot interference. Inset: square root of the absorbance as a function of energy. Linear extrapolation of the square root of absorbance reveals an optical gap of 0.77 eV associated with an indirect bandgap material. b) Micro-PL spectra show that the peak intensity decreases over exposure time to air. c) Corresponding micro-Raman spectra show the emergence of two Raman peaks after sample exposure to air (each indicated by an asterisk for the spectrum measured after one week).

to pristine GaTe. No change was observed either in crystals stored for extended periods in either dry air or water-vapor-saturated nitrogen gas. Further, as-cleaved GaTe submersed in deionized water displays a strong dependence on the concentration of dissolved oxygen in water. A lower level of oxygen dissolved in the water leads to a slower rate of change in optical properties (see Figure S1, Supporting Information). Therefore, the spectral changes reported here require both oxygen and water. Oxidation of layered black phosphorus has been found to require both oxygen and water (and light).[29] However unlike black phosphorus, which roughens due to decomposition from oxidation, GaTe remains smooth and layered after extended exposure to air as reflected by only a small increase in root mean square (RMS) roughness from 0.3 to 0.7 nm. Based on these observations, we focus on a picture for GaTe whereby exposure to air induces a transformation into a disordered phase (henceforth referred to as GaTe—O_2) in which oxygen chemisorbs to tellurium.

We used X-ray photoelectron spectroscopy (XPS) of air-exposed samples to identify possible changes in the oxidation state of Ga and Te (see Figure S2, Supporting Information). Spectra show the partial oxidation of Te and Ga similar to reports of Balitskii et al.[30,31] This can be attributed to the formation of a native oxide at the surface and/or to the participation of oxygen in the proposed transformation. Importantly, even upon extended exposure to air, the peaks associated with unoxidized Te (at 583.5 and 573.5 eV) persist. Additionally, Hall effect and resistivity measurements indicate that the electrical properties are similar after the transformation. We have exfoliated crystals (from many microns down to 20 nm in thickness) that have transformed fully. Measuring a fully transformed sample, we find that it remains p-type with a hole concentration and mobility of 9×10^{15} cm^{-3} and 17 cm^2 V^{-1} s^{-1}, respectively. Thus, while surface oxides may be present, the observed electrical and optical properties cannot be explained by them alone.

The structural changes in GaTe as a function of exposure time were studied by X-ray diffraction (XRD). The crystals were oriented with the $\{\bar{2}\ 0\ 1\}$ family of planes scattering in the instrument's out-of-plane direction. Given the layered nature of GaTe, we expect these planes to demonstrate the greatest structural change should species from air incorporate between layers. As a result, we focused on the most intense peak of this family, the $(\bar{4}\ 0\ 2)$ peak.

For a fully transformed sample the $(\bar{4}\ 0\ 2)$ peak displays a diffraction intensity one order of magnitude lower than as-cleaved GaTe (**Figure 2**a). The loss in intensity is indicative of some structural transformation. Simultaneously, the $(\bar{4}\ 0\ 2)$ peak of the fully transformed sample is shifted to smaller 2θ values by 0.01°, suggesting that the transformation results in a small increase in interplanar spacing. High-resolution XRD scans of the $(\bar{4}\ 0\ 2)$ peak in multiple samples were measured as a function of sample exposure time to air. The data demonstrate a clear increase in the out-of-plane lattice spacing that reaches a lattice strain as high as 0.2% (Figure 2b). This suggests the incorporation of species between GaTe layers, expanding the lattice in the $[\bar{2}\ 0\ 1]$ direction.

To better visualize the reason for the loss in the $(\bar{4}\ 0\ 2)$ diffraction intensity, reciprocal space maps in samples of different exposure times to air were obtained (Figure 2c–e). Reciprocal space maps provide additional information about the orientation of the surface (ω) and distribution of lattice spacing within the crystal (2θ). We observed broadening of the surface orientation with increasing exposure time, creating an almost bimodal distribution after one year. Such a redistribution of orientation signifies typically an increase in structural disorder as well as buckling or rippling. Finally, XRD characterization confirms that the Te—O bonds observed by XPS cannot be attributed exclusively to the presence of a TeO_2 phase (Figure S3, Supporting Information).

The effect of oxygen chemisorption on the properties of GaTe has been explored by density functional theory (DFT). We begin with pristine GaTe followed by GaTe—O_2, GaTe—H_2O and GaTe—OH. The calculated bandstructure of GaTe has a direct bandgap of 1.72 eV at the M-point (**Figure 3**a). This value is still below the extrapolated 1.8 eV at 0 K[12] but is a better approximation than those reported elsewhere.[32–34] The contribution of the orbitals to the partial density of states (PDOS) of GaTe can be seen in Figure S4a (Supporting Information). In addition, the GaTe Raman-active modes were calculated and agree with our experimental data (see Figure S5, Supporting Information) as well as published values.[26,27]

© 2016 WILEY-VCH Verlag GmbH & Co. KGaA, Weinheim

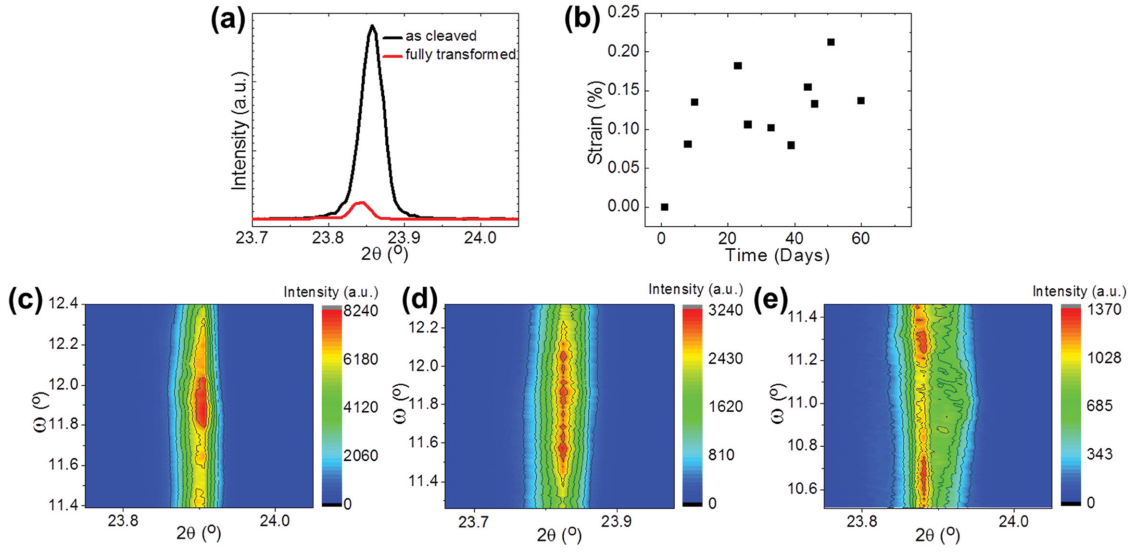

Figure 2. a) ($\bar{4}$ 0 2) X-ray diffraction peak before (black) and after (red) sample transformation in air. b) Lattice strain along the *c*-plane as a function of time for several samples. Reciprocal space maps of the ($\bar{4}$ 0 2) diffraction peak for c) as-cleaved sample, d) sample exposed to air for three weeks, and e) for one year.

For the optimized GaTe—O_2 structure, we find that O_2 binds preferentially to the Te atoms whose lone pairs are less hindered (perpendicular to the layer) as depicted in Figure 3b. Isosurface charge density of GaTe—O_2 for a plane passing through the oxygen atoms and their nearest neighbor Te clearly shows the interaction between GaTe and O_2. In order to simplify the calculations, one chemisorbed oxygen molecule was added to each unit cell (GaTe—O_2) although a less-concentrated random distribution of oxygen molecules could be expected. Figure 3c,d shows the corresponding bandstructure and PDOS for GaTe—O_2 (for better details in the PDOS see Figure S4b in the Supporting Information); a significant restructuring of the conduction band takes place. The new conduction band minimum is now located at the Γ-point, making GaTe—O_2 a semiconductor with an indirect bandgap of 0.86 eV. While it is rather fortuitous that the calculated gap for GaTe and GaTe—O_2 match remarkably well with the measured gaps, we focus on the consistency of the calculated and experimental bandgaps in indicating a transformation from direct to indirect and a reduction in the magnitude by about half. Further, although we expect that oxygen molecules chemisorb randomly over a Te-terminated surface, the salient features of our calculations are not expected to change with such randomness.

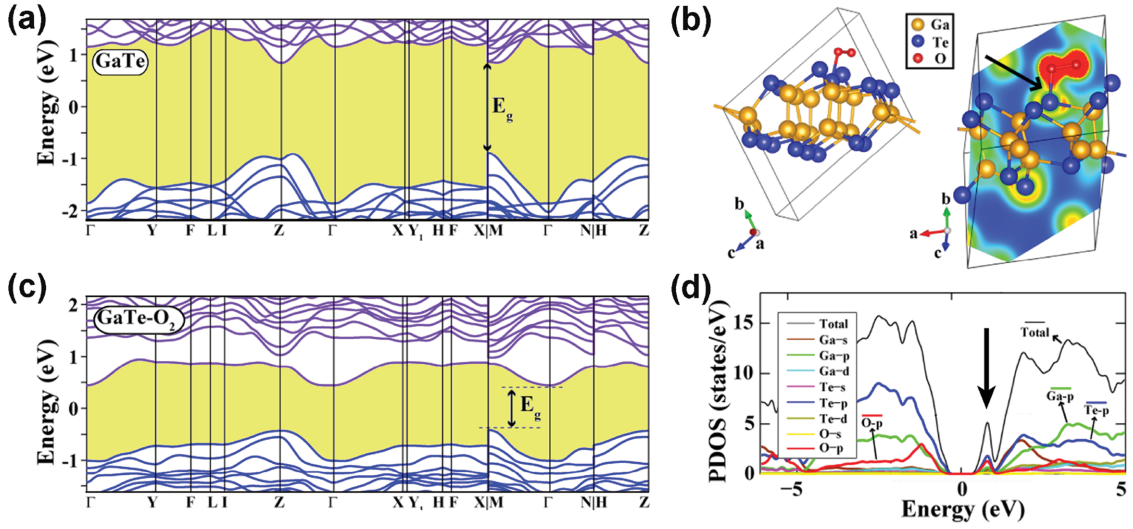

Figure 3. a) Calculated bandstructure of monoclinic GaTe along high-symmetry lines. Bandgap as a function of direction is shaded. The zero of energy was set to Fermi level. Calculations were performed in 2 × 1 × 1 supercell. b) Atomic structure and charge density profile of oxygen molecule chemisorbed to GaTe. The new bond formed between a Te atom and an oxygen molecule is indicated by an arrow. c) Calculated band structure for O_2-chemisorbed GaTe. d) Total and orbital-projected density of states of GaTe—O_2 near the band gap, showing the new conduction sub-band.

© 2016 WILEY-VCH Verlag GmbH & Co. KGaA, Weinheim

As shown in Figure 3d, the hybridization of the O 2p states with the valance orbitals in GaTe contributes to the formation of two new sub-bands associated with the conduction band. These two new sub-bands are most relevant in giving GaTe—O_2 its distinct optical properties. The low-lying sub-band, which gives rise to the new conduction band minimum at the Γ-point, is composed mainly of Te 5p and O 2p states. Because oxygen chemisorption most strongly affects the conduction band, the oxygen-chemisorbed phase displays electrical *p*-type properties similar to as-exfoliated GaTe. We note that DFT calculations for GaTe—H_2O did not reveal any major changes in the bandstructure of GaTe, while calculations for GaTe—OH (i.e., Te binding a hydroxyl group) reveal a metallic phase (see Figure S4c,d in the Supporting Information). However, fully transformed samples remain semiconducting; their electrical resistance increases by more than an order of magnitude upon cooling from room temperature to 160 K. This electrical behavior is consistent with a semiconducting GaTe—O_2 rather than metallic GaTe—OH phase.

The Raman-active modes of GaTe—O_2 were also calculated. Three of the Raman-active modes found, located around 130, 146, and 183 cm^{-1}, are in excellent agreement with the three Raman peaks observed in the samples after the transformation (see Figure S5 in the Supporting Information). The measured peaks are broad, suggesting that oxygen induces a high level of disorder even as the transformed film remains layered. This is consistent with XRD as discussed above.

If a species such as oxygen has been adsorbed between the layers of GaTe, one may expect thermal annealing to drive out such species thus restoring the properties of the sample to its as-cleaved state. To probe this possibility we annealed transformed samples at 300 °C for 5 min in a nitrogen atmosphere. Such annealing results in the formation of bubble-like features (**Figure 4**a,c) that are not observed in as-cleaved crystals that received the same thermal treatment (Figure 4b,d) (and Figure S6, Supporting Information). In the proposed scenario—in which O_2 chemisorbs to Te—bubbles may form by the unbinding and collection of O_2 present between the GaTe layers. We find that prolonged annealing indeed causes the localized, partial reversal of the transformation, specifically near edges, steps and bubbles that have burst. Measurement of the PL spectrum in the vicinity of a bubble that burst via extended annealing (450 °C for 12 h in an argon atmosphere) reveals a partial recovery of the 1.65 eV peak that decreases in intensity with distance away from the burst bubble (Figure 4e,f). The formation of the bubbles and the partial reversal around the burst ones further support the picture of the incorporation of a molecule like oxygen between the layers that modifies the bandstructure of the GaTe host.

In summary, under typical ambient conditions multilayer GaTe should be treated as a narrow-gap semiconductor. We propose that the transformation of GaTe from a material with a 1.65 eV bandgap to one with a bandgap below 0.8 eV originates from the incorporation and chemisorption of oxygen to tellurium. The reversible surface-mediated electronic transformation in GaTe reported here is akin to that achieved irreversibly in conventional semiconductors by alloying and demonstrates a paradigm for bandgap engineering that is accessible in layered chalcogenides through the rational design of adsorbates and their hybridization with surface atoms.

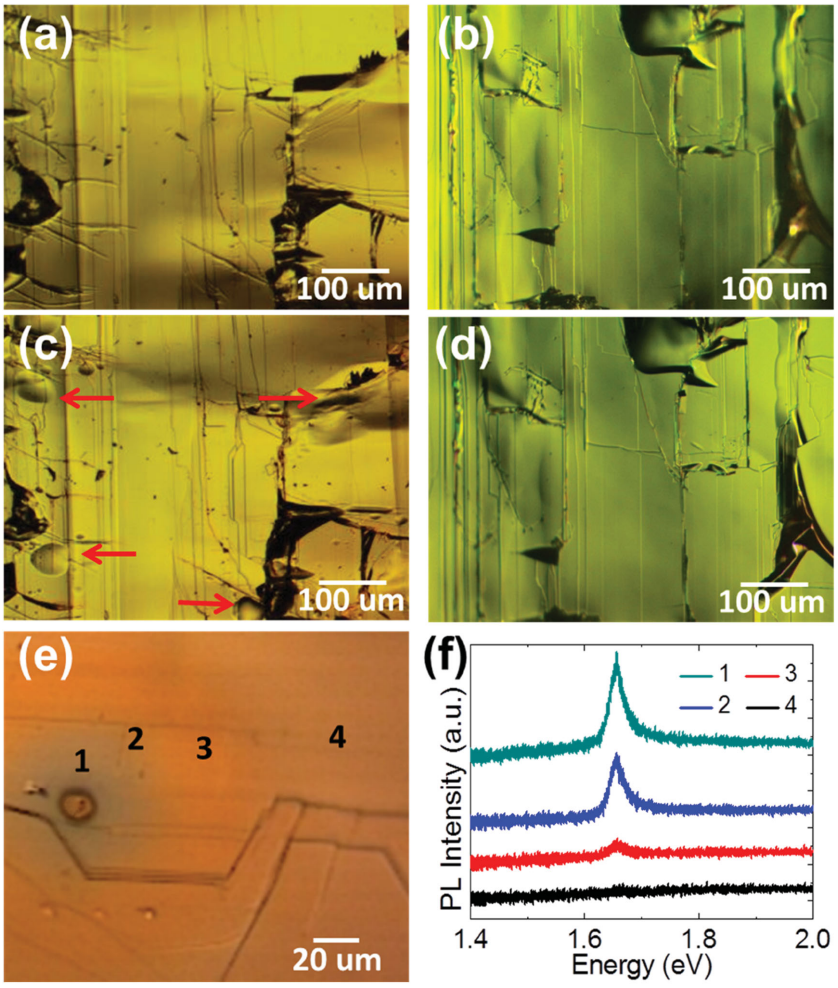

Figure 4. Optical microscopy image of a) transformed and b) as-cleaved flakes of GaTe. c) Optical microscopy image of (a) after rapid thermal annealing at 300 °C for 5 min in nitrogen. Several bubbles under the surface (indicated with red arrows in (c)) were formed during thermal annealing. d) Optical microscopy image of (b) after rapid thermal annealing under the same conditions as (c). No major change is observed. e) Optical microscopy image of an area around a bubble that formed and burst upon annealing. The burst bubble is surrounded by a green "halo". f) Micro-PL spectra in different regions near the burst bubble in (e). The increase in the relative PL intensity confirms the recovery of GaTe after annealing. The radius of the PL spot was 1.3 μm.

© 2016 WILEY-VCH Verlag GmbH & Co. KGaA, Weinheim

Experimental Section

Sample Preparation and Characterization: Gallium telluride samples were produced from millimeter thick single crystals by exfoliation using tape or by peeling with a razor blade. Repeating these procedures, we obtained flakes with fresh surfaces on both sides. For samples stored in water, the removal of oxygen from water was performed using a prescribed process.[35] Nitrogen gas was bubbled through deionized water for at least 45 min before samples were placed in it; the bubbling of nitrogen gas was then maintained to achieve the less oxygenated environment. The oxygen content of the water was measured using a dissolved oxygen meter before and after the introduction of samples.

The samples were investigated over time by optical absorption and photomodulated reflectance spectroscopies. Raman and PL spectroscopies were performed using a laser wavelength of 488 nm. XPS was carried out using a nonmonochromatic Al Kα X-ray source (1486.6 eV) and a hemispherical-type multichannel analyzer in vacuum (base pressure of $\approx 1 \times 10^{-10}$ Torr). The binding energies are referenced by direct electrical contact to the Fermi energy of the spectrometer whose work function is 4.5 eV. Hall effect measurements were performed with a magnetic field of 0.6 T. Samples were prepared in a van der Pauw geometry with Cr/Au contacts. The rapid thermal annealing of samples was carried out at 300 °C for 5 min in a nitrogen atmosphere, while the extended thermal annealing was carried out at 450 °C for up to 12 h in argon. All electrical and optical measurements were performed at room temperature.

First-Principles Calculations: First-principles calculations were performed in the framework of DFT. Structural relaxations and phonon calculations were carried out using the well-known Perdew–Burke–Ernzerhof (PBE) exchange-correlation functional including van der Waals corrections.[36,37] For band structure and density of states calculations, we used the Heyd–Scuseria–Ernzerhof (HSE) functional which is a screened hybrid functional introduced by Heyd, Scuseria, and Ernzerhof.[38] One quarter of the PBE short-range exchange was replaced by exact exchange while the full PBE correlation energy was included. This hybrid functional was shown to yield improved band gaps compared to PBE functional.[39] The interaction between the ions and valence electrons are described by the projected augmented wave method with a plane wave cutoff of 340 eV.[40] Brillouin-zone integrations were performed using $(4 \times 4 \times 4)$ Monkhorst-Pack grids. All atomic positions and lattice constants were optimized using the conjugate gradient method in which total energy and atomic forces are minimized. Effects of oxygen intercalation were simulated by adding an oxygen molecule into $2 \times 1 \times 1$ supercell of monoclinic GaTe structure (which we denote henceforth as GaTe—O_2) containing 12 Ga and 12 Te atoms. The same simulation cell was retained for pristine GaTe. The character of phonon modes, whether Infrared (IR) or Raman active, was determined according to IR-active mode intensities. DFT calculations were performed using Vienna Ab-initio Simulation Package (VASP) code.[41]

Supporting Information

Supporting Information is available from the Wiley Online Library or from the author.

Acknowledgements

J.J.F. acknowledges the support from the National Science Foundation Graduate Research Fellowships Program (Grant No. DGE-1106400). Experiments were supported by the Electronic Materials Program (EMAT). XPS at the Molecular Foundry and EMAT were funded by the Director, Office of Science, Office of Basic Energy Sciences, and Materials Sciences and Engineering Division of the U.S. Department of Energy under Contract No. DE-AC02-05CH11231. The authors gratefully acknowledge Dr. D. Frank Ogletree for the assistance with the XPS and O. Olukoya for initial experiments on exfoliating GaTe. Computational resources were partly provided by TUBITAK ULAKBIM, High Performance and Grid Computing Center (TR-Grid e-Infrastructure). Part of this work was performed at the Stanford Nano Shared Facilities (SNSF).

Received: February 27, 2016
Revised: April 14, 2016
Published online: May 12, 2016

[1] K. F. Mak, C. Lee, J. Hone, J. Shan, T. F. Heinz, *Phys. Rev. Lett.* **2010**, *105*, 136805.
[2] B. Radisavljevic, A. Radenovic, J. Brivio, V. Giacometti, A. Kis, *Nat. Nanotechnol.* **2011**, *6*, 147.
[3] S. Tongay, S. S. Varnoosfaderani, B. R. Appleton, J. Wu, A. F. Hebard, *Appl. Phys. Lett.* **2012**, *101*, 123105.
[4] S. Tongay, J. Zhou, C. Ataca, K. Lo, T. S. Matthews, J. Li, J. C. Grossman, J. Wu, *Nano Lett.* **2012**, *12*, 5576.
[5] D. V. Rybkovskiy, N. R. Arutyunyan, A. S. Orekhov, I. A. Gromchenko, I. V. Vorobiev, A. V. Osadchy, E. Y. Salaev, T. K. Baykara, K. R. Allakhverdiev, E. D. Obraztsova, *Phys. Rev. B* **2011**, *84*, 085314.
[6] P. Hu, Z. Wen, L. Wang, P. Tan, K. Xiao, *ACS Nano* **2012**, *6*, 5988.
[7] J.-Y. Kim, S.-M. Choi, W.-S. Seo, W.-S. Cho, *Bull. Korean Chem. Soc.* **2010**, *31*, 3225.
[8] J. C. Irwin, R. M. Hoff, B. P. Clayman, R. A. Bromley, *Solid State Commun.* **1963**, *13*, 1531.
[9] D. J. Late, B. Liu, J. Luo, A. Yan, H. S. S. R. Matte, M. Grayson, C. N. R. Rao, V. P. Dravid, *Adv. Mater.* **2012**, *24*, 3549.
[10] D. J. Late, B. Liu, H. S. S. R. Matte, C. N. R. Rao, V. P. Dravid, *Adv. Funct. Mater.* **2012**, *22*, 1894.
[11] J. L. Brebner, G. Fischer, E. Mooser, *J. Phys. Chem. Solids* **1962**, *23*, 1417.
[12] C. Tatsuyama, Y. Watanabe, C. Hamaguchi, *J. Phys. Soc. Japan1* **1970**, *29*, 150.
[13] G. Yu, Z. Liu, X. Xie, X. Ouyang, G. Shen, *J. Mater. Chem. C* **2014**, *2*, 6104.
[14] P. Hu, J. Zhang, M. Yoon, X. F. Qiao, X. Zhang, W. Feng, P. Tan, W. Zheng, J. Liu, X. Wang, J. C. Idrobo, D. B. Geohegan, K. Xiao, *Nano Res.* **2014**, *7*, 694.
[15] Z. Wang, K. Xu, Y. Li, X. Zhan, M. Safdar, Q. Wang, F. Wang, J. He, *ACS Nano* **2014**, *8*, 4859.
[16] C. Rocha Leão, V. Lordi, *Phys. Rev. B* **2011**, *84*, 165206.
[17] K. C. Mandal, R. M. Krishna, T. C. Hayes, P. G. Muzykov, S. Das, T. S. Sudarshan, S. Ma, *IEEE Trans. Nucl. Sci.* **2011**, *58*, 1981.
[18] S. A. Semelitov, V. A. Vlasov, *Sov. Phys. Crystallogr.* **1964**, *8*, 704.
[19] E. G. Gillan, A. R. Barron, *Chem. Mater.* **1997**, *9*, 3037.
[20] O. A. Balitskii, B. Jaeckel, W. Jaegermann, *Phys. Lett. A* **2008**, *372*, 3303.
[21] N. N. Kolesnikov, E. B. Borisenko, D. N. Borisenko, A. V. Timonina, *J. Cryst. Growth* **2013**, *365*, 59.
[22] M. Abdel Rahman, A. E. Belal, *J. Phys. Chem. Solids* **2000**, *61*, 925.
[23] M. Mohil, G. A. Kumar, *J. Nano- Electron. Phys.* **2013**, *5*, 02018.
[24] V. M. Bermudez, *Chem. Phys.* **2006**, *323*, 193.
[25] F. Cerdeira, E. A. Meneses, A. Gouskov, *Phys. Rev. B* **1977**, *16*, 1648.
[26] G. B. Abdullaev, L. K. Vodopyanov, K. R. Allakhverdiev, L. V. Golubev, S. S. Babaev, E. Y. Salaev, *Solid State Commun.* **1979**, *31*, 851.
[27] J. C. Irwin, B. P. Clayman, D. G. Mead, *Phys. Rev. B* **1979**, *19*, 2099.
[28] K. C. Mandal, T. Hayes, P. G. Muzykov, R. Krishna, S. Das, T. S. Sudarshan, S. Ma, *Proc. SPIE* **2010**, *7805*, 78050Q1.
[29] A. Favron, E. Gaufres, F. Fossard, A.-L. Phaneuf-L'Heureux, Y.-W. Tang, P. L. Levesque, A. Loiseau, R. Leonelli, S. Francoeur, R. Martel, *Nat. Mater.* **2015**,*14*, 826.
[30] O. A. Balitskii, *Mater. Lett.* **2006**, *60*, 594.
[31] O. A. Balitskii, W. Jaegermann, *Mater. Chem. Phys.* **2006**, *97*, 98.

© 2016 WILEY-VCH Verlag GmbH & Co. KGaA, Weinheim

[32] A. Yamamoto, A. Syouji, T. Goto, E. Kulatov, K. Ohno, Y. Kawazoe, K. Uchida, N. Miura, *Phys. Rev. B* **2001**, *64*, 035210.
[33] J. F. Sánchez-Royo, J. Pellicer-Porres, A. Segura, V. Muñoz-Sanjosé, G. Tobías, P. Ordejón, E. Canadell, Y. Huttel, *Phys. Rev. B* **2002**, *65*, 115201.
[34] Z. Rak, S. D. Mahanti, K. C. Mandal, N. C. Fernelius, *J. Phys. Condens. Matter* **2009**, *21*, 015504.
[35] I. B. Butler, M. A. Schoonen, D. T. Rickard, *Talanta* **1994**, *41*, 211.
[36] J. Perdew, K. Burke, M. Ernzerhof, *Phys. Rev. Lett.* **1996**, *77*, 3865.
[37] S. Grimme, *J. Comput. Chem.* **2006**, *27*, 1787.
[38] J. Heyd, G. E. Scuseria, M. Ernzerhof, *J. Chem. Phys.* **2006**, *124*, 219906.
[39] K. Hummer, J. Harl, G. Kresse, *Phys. Rev. B* **2009**, *80*, 115205.
[40] G. Kresse, D. Joubert, *Phys. Rev. B* **1999**, *59*, 1758.
[41] G. Kresse, J. Hafner, *Phys. Rev. B* **1993**, *47*, 558(R).

© 2016 WILEY-VCH Verlag GmbH & Co. KGaA, Weinheim